Xu et al. Nanoscale Research Letters (2017) 12:54
DOI 10.1186/s11671-017-1834-1

Nanoscale Research Letters

NANO EXPRESS Open Access

Ag Nanoparticles Located on Three-Dimensional Pine Tree-Like Hierarchical TiO_2 Nanotube Array Films as High-Efficiency Plasmonic Photocatalysts

Jinxia Xu[1,2], Zhenhuan Wang[2], Wenqing Li[1], Xingang Zhang[1], Dong He[1] and Xiangheng Xiao[1,3*]

Abstract

High specific surface area three-dimensional pine tree-like hierarchical TiO_2 nanotube array films loaded with Ag nanoparticles were successfully prepared by one-step hydrothermal reaction combining with simple and feasible magnetron sputtering. The composite Ag/TiO_2-branched nanotube arrays show outstanding photocatalytic property, which is attributed to the boost of plasmonic enhancement carrier generation and separation, higher specific surface area, higher organic pollutant absorption, faster charge transport, and superior light-harvesting efficiency for efficient charge collection. The work provides a cost-effective and flexible pathway to develop high-performance photocatalyst or optoelectronic devices.

Keywords: Three-dimensional TiO_2, Ag nanoparticles, Plasmonics, Photocatalysts

Background

In spite of nearly half a century investigations, since Fujishima and Honda discovered the photocatalytic water splitting on TiO_2 electrodes in 1972 [1], TiO_2 still remains to be intensively investigated as semiconductor photocatalyst owing to its important applications in phtocatalysis [2–7], photoelectrochemical water splitting [8–12], solar cell [13–16], and sensors [17, 18], because of its excellent chemical stability, abundance, and low cost. However, the photocatalytic activities of TiO_2 are restricted by its low photocatalytic sensitivity in the UV region and rapid recombination of photogenerated electron and hole pairs [19]. Much effort has been dedicated to enhance the photocatalytic efficiency of TiO_2 in the aspect of morphology, surface area, and surface defects. Zero-dimensional (D) TiO_2 particles fabricated with randomly organized provides a large specific surface area for absorbing sufficient dye molecules. However, it has high charge recombination because of the large grain boundary of nanoparticles (NPs) [20, 21]. Then, well-aligned one-dimensional nanostructure such as nanowires, nanorods, and nanotubes were fabricated to improve charge transport due to a direct transport pathway for photogenerated electrons [22–24]. Nevertheless, the drawback of the low surface-to-volume ratio of one-dimensional nanostructure results to a low photocatalytic activity. Recently, researchers have been enthusiastically dedicated to develop three-dimensional nanostructures such as nanoflowers and nanotrees for application in photocatalysis [25–28]. Compared with zero-dimensional NPs and one-dimensional nanowires, the three-dimensional nanostructure offers the advantage of a large surface area that increases dye loading. Additionally, the three-dimensional morphology could offer long optical paths for efficient light absorption and abundant active sites for electrochemical reactions, providing efficient transport pathway for rapid charge transport that leads to improving electron collection and electron-hole separation.

TiO_2 decorated with noble metal (Au, Ag, Pt, etc.) NPs named plasmonic photocatalysis is another promising

* Correspondence: xxh@whu.edu.cn
[1]Department of Physics and Key Laboratory of Artificial Micro- and Nano-Structures of Ministryof Education and Laboratory of Printable Functional Nanomaterials, Wuhan University, Wuhan 430072, People's Republic of China
[3]Su Zhou Institute of Wuhan University, Suzhou 215123, People's Republic of China
Full list of author information is available at the end of the article

method for enhancing the photocatalytic activity of TiO_2 owing to the localized surface plasmon resonance (LSPR) effect of metal NPs [29–33]. The band gap of TiO_2 is about 3.2 eV, and Ag NPs show a very strong LSPR absorption in the near-UV region [34, 35]. So, Ag is an optimal choice due to the Ag NPs' LSPR position close to the exciton absorption of TiO_2; on the other hand, silver is most suitable for industrial applications owing to its easy preparation and low cost. Moreover, the Ag NPs decorated on the surface of TiO_2 could act as an electron trap center to effectively prevent electron-hole recombination and enhance the photocatalytic activity.

Herein, we report a high-performance plasmonic photocatalyst three-dimensional pine tree-like hierarchical TiO_2 nanotube array films loaded with Ag NPs fabricated by a simple two-step process. The composite Ag/TiO_2-branched nanotube arrays show outstanding photocatalytic property, which is attributed to the boost of plasmonic-enhanced carrier generation and separation, higher specific surface area, higher organic pollutant absorption, faster charge transport, and superior light-harvesting efficiency for efficient charge collection. Figure 1 illustrates the formation procedure and proposed photocatalytic mechanism of three-dimensional pine tree-like hierarchical TiO_2 nanotube array films loaded with Ag NPs. Compared with our previous work, the photocatalytic activity of three-dimensional pine tree-like hierarchical TiO_2 nanotube array films loaded with Ag NPs was further enhanced.

Results and Discussion

The microstructural and morphology detail of the prepared three-dimensional pine tree-like hierarchical TiO_2 nanotube arrays is shown in Fig. 2a. The cross-sectional SEM images show that the prepared three-dimensional pine tree-like hierarchical TiO_2 nanotube arrays composing of a vertically oriented nanotube trunk with a length of approximately 5 μm grafted with large amounts of short branches with lengths of about 300 nm were directly grown on FTO substrate by a simple one-step hydrothermal method. As shown in Fig. 2b the SEM image and magnified image (the inset) of three-dimensional pine tree-like hierarchical TiO_2 nanotube arrays, the three-dimensional TiO_2 nanotube arrays were fully covered and arranged homogeneously on the FTO glasses with large-scale and uniform growth and large amounts of short nanorod branches. The magnified image shows the diameter of the branch at approximately 50 nm. This hierarchical architecture with large specific surface area can enhance the absorption of dye molecules and effectively improve charge transport by a direct transport path thereby may be improving the photocatalytic activity of the TiO_2. The phase purity and structure of the three-dimensional pine tree-like hierarchical TiO_2 nanotube arrays were analyzed using XRD as shown in Fig. 2c. It can be found that diffraction peaks appeared at 25.4° and 48°, which can be attributed to the (101) and (200) orientations of the anatase TiO_2 (JCPDS No.21-1272) [36]. No characteristic peak of any impurity is probed, which demonstrates that the sample fabricated by this method has high phase purity. Raman scattering as a local probe is very sensitive to microstructures and crystallinity of materials. Figure 2d shows the Raman scattering spectra of three-dimensional pine tree-like hierarchical TiO_2 nanotube arrays. The founded Raman bands at 145, 399, 516, and 640 cm^{-1} can be separately indexed to the Eg, B1g, A1g, or B1g and Eg, which are consistent with the anatase phase of TiO_2 and without any signal of a brookite or rutile phase [37, 38]. This result is consistent with the XRD. All the results show that the three-dimensional pine tree-like hierarchical anatase TiO_2 nanotube array films were successfully fabricated.

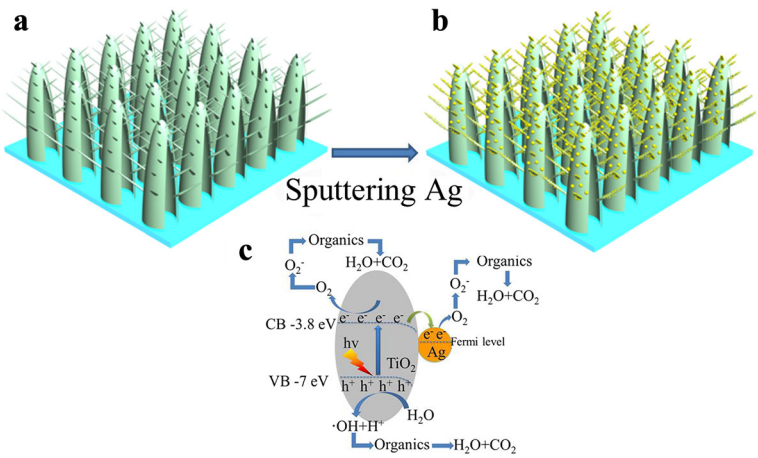

Fig. 1 **a**, **b** Schematic illustration of the formation of Ag-decorated three-dimensional pine tree-like hierarchical TiO_2 nanotube arrays. **c** Schematic illustration of the photogenerated electron transfer process in Ag/TiO_2 comoposite under UV and visible light irradiation

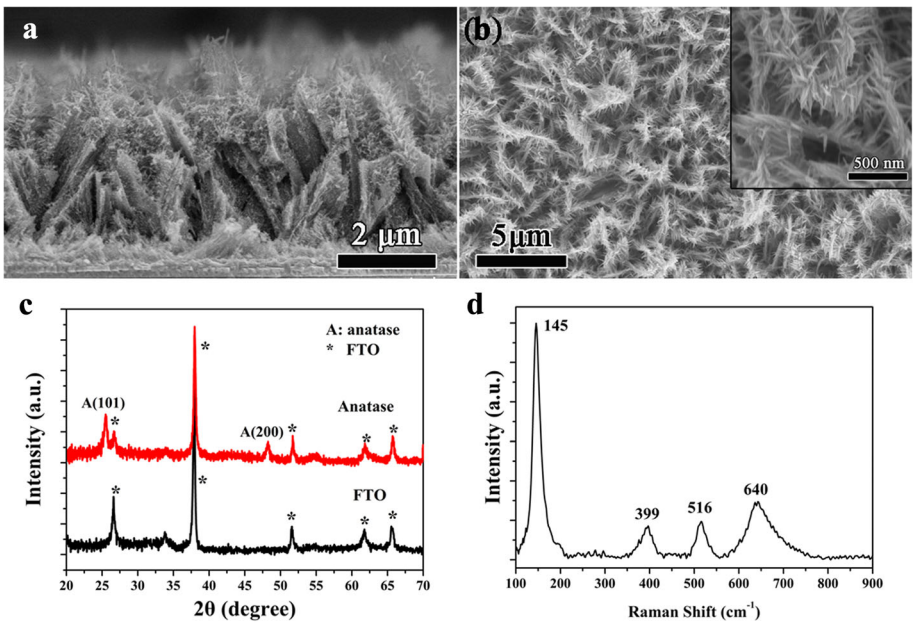

Fig. 2 **a** Cross-sectional SEM image, **b** SEM image and magnified image (the inset), **c** XRD pattern, and **d** Raman spectrum of three-dimensional pine tree-like hierarchical TiO_2 nanotube arrays

The typical SEM views of Ag NPs with deposition time of 10, 20, 30, and 40 s are shown in Fig. 3a–d, and the inset one is the corresponding magnified image. It can be observed that Ag NPs are uniformly coated on the branches of TiO_2. The mean diameter of Ag NPs is approximately13, 25, 35, and 45 nm in sample Ag(10s)/TiO_2, Ag(20s)/TiO_2, Ag(30s)/TiO_2, and Ag(40s)/TiO_2, respectively. It is obvious that the diameter of Ag NPs increases with the increase of silver deposition time. So, Ag NPs deposited uniformly on three-dimensional pine tree-like hierarchical TiO_2 nanotube arrays by a simple magnetron sputtering system were fabricated. It is well know that the LSPR effect of Ag NPs can form a strong local electronic field. Moreover, Ag NPs here were decorated uniformly on the branches of TiO_2, so the near-field dipolar interactions between adjacent particles [39] were very strong. Therefore, it may form a stronger local electronic field in the hierarchical structure. So, Ag NPs deposited on three-dimensional pine tree-like hierarchical TiO_2 nanotube arrays are expected with higher performance.

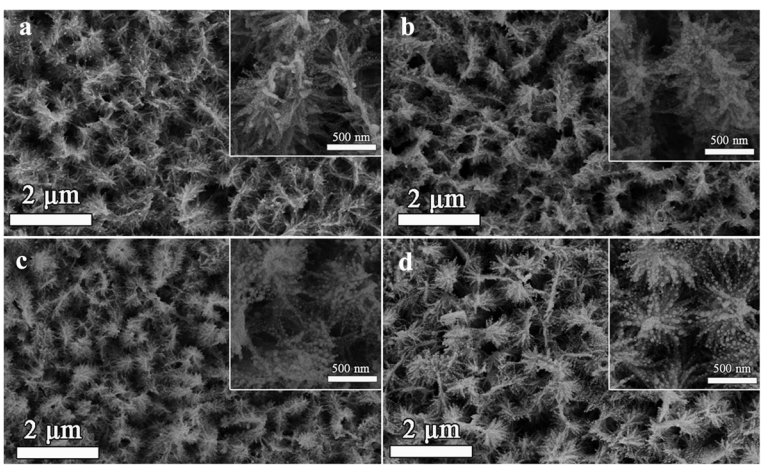

Fig. 3 SEM images of three-dimensional pine tree-like hierarchical TiO_2 nanotube arrays deposited with Ag by different deposition times: **a** 10 s, **b** 20 s, **c** 30 s, and **d** 40 s, and the set one is the corresponding magnified image

To further demonstrate the successful fabrication of Ag NPs deposited on three-dimensional pine tree-like hierarchical TiO_2 nanotube arrays, the elemental chemical status and compositions of Ag(30s)/TiO_2 were analyzed by XPS. Figure 4a shows the XPS spectrum of Ti 2p. It can be observed that two peaks at binding energies of 464.3 and 458.5 eV can be attributed to Ti $2p_{3/2}$ and Ti $2p_{1/2}$, respectively. The result demonstrates the state of Ti^{4+} in the anatase TiO_2 [40]. The O 1s peaks at binding energy of 529.8 eV are attributed to the typical signal of Ti-O-Ti as shown in Fig. 4b [41]. The Ag 3d XPS spectrum shown in Fig. 4c consists of two peaks at 368.1 and 374.1 eV with a distance of approximately 6.0 eV. These binding energies are consistent with Ag $3d_{5/2}$ and Ag $3d_{3/2}$, confirming that Ag NPs primarily exist in the metallic form in the Ag/TiO_2 composite [42].

The technique to characterize the plasmonic response absorption of Ag NPs is to investigate the UV-vis absorption spectrum. At Ag LSPR frequency, Ag NPs exhibit strong absorption. Figure 5 displays the absorption spectra of TiO_2 and Ag NPs deposited on the branches of TiO_2 with different deposited times. The absorption edge nearby 400 nm belongs to the optical band gap absorption of TiO_2 [43]. The increased absorption peak at around 425 nm belongs to the SPR of Ag NPs. It also shows that absorption peak increases with the increase of Ag NPs on the surface of TiO_2. It can be observed that the position of Ag NPs SPR is close to the exciton absorption of TiO_2. Hence, it is beneficial for the energy coupling of the TiO_2 plasmonic photocatalyst.

The phototcatalytic activity of TiO_2 array films, Ag(10s)/TiO_2, Ag(20s)/TiO_2, Ag(30s)/TiO_2, and Ag(40s)/TiO_2 composite systems with an area about 6 cm^2 was evaluated by degradation of the rhodamine B (RhB) solution under UV and visible irradiation, and the temperature was maintained at 18 °C in the process of photocatalytic reaction (Table 1). And the RhB solution was also measured under the same experimental conditions. The irradiation time interval is 30 min. As shown in Fig. 6a, the concentration of RhB is decreased upon the irradiation time. The RhB decolorization rate for the three-dimensional pine tree-like hierarchical TiO_2 nanotube can only approach 55% after 2-h UV-vis light irradiation. However, it is found that the photocatalytic efficiency of the Ag/TiO_2 composite films increases significantly than the pure TiO_2. The Ag(30s)/TiO_2 shows the highest photocatalytic performance that degraded 98% of RhB after the UV-vis light irradiation for 1 h. The degradation of Ag(20s)/TiO_2 is 96% after 1.5-h UV-vis light irradiation. The degradation of Ag(10s)/TiO_2 is 98%, and the degradation of Ag(40s)/TiO_2 is 84% after 2-h UV-vis light irradiation. Moreover, the photocatalytic reaction of semiconductor materials can be accounted for by Langmuir-Hinshelwood (L-H) model, The L-H model equation is as below [44]:

$$\ln(A_0/A) = kt$$

where A_0/A represents the ratio of concentration of the dye at adsorption-desorption equilibrium and after irradiation for time t. And the k is the apparent first-order reaction rate constant (min^{-1}). The k value of TiO_2 and Ag/TiO_2 composite structure with different Ag deposition times are shown in Table 2. The k value of pure TiO_2 is 9×10^{-3} min^{-1}, and the Ag(30s)/TiO_2 shows that the largest k value is about 6×10^{-2} min^{-1}. The k value of Ag(30s)/TiO_2 is nearly seven times than that of pure TiO_2, and the k value of other samples is 3.7×10^{-2} min^{-1}(Ag(20s)/TiO_2), 3.5×10^{-2} min^{-1}(Ag(10s)/TiO_2), and 1.5×10^{-2} min^{-1} (Ag(40s)/TiO_2). The enhancement of the photocatalytic efficiency is significant for all Ag deposited samples than the pure TiO_2, and the photocatalytic efficiency of Ag/TiO_2 is increased with the increase of Ag deposition time, but with further increase of the deposition time to 40 s, the sample shows lower photocatalytic efficiency than other samples. Therefore, the optimum Ag deposition time is 30 s in the research.

The stability of the photocatalyst is very important for practical applications. Therefore, the stability of Ag(30s)/TiO_2 has been further evaluated by recycling the photocatalyst for RhB degradation as shown in Fig. 6b. It can be seen that the degradation rate of RhB solution is more than 90% after 4 cycles with duration of 60 min per cycle, which is to say that the photocatalytic efficiency of Ag(30s)/TiO_2 does not exhibit obvious loss after several recycles. The result shows that the Ag/TiO_2 composite has high stability during the photocatalytic degradation of RhB.

On the basis of the experiment results, the outstanding photocatalytic performance of Ag/TiO_2 may be explained as follows:

(1) Large specific surface area and fast charge transport. Three-dimensional pine tree-like hierarchical TiO_2 nanotube arrays composing of a vertically oriented nanotube trunks and grafted with large amounts of short branches that have a large surface and enhance the absorption of dye molecules. Moreover, the photo-induced electrons directly transport through the nanotube [45], and the nanotube provides efficient transport pathway for rapid charge transport that leads to improving the electron collection and the electron-hole separation. Therefore, the photocatalytic activity of TiO_2 could be increased.

(2) LSPR-mediated local field enhancement. It is well known that the LSPR effect of Ag NPs can induce a strong local electric field. Moreover, here, a large number of Ag NPs are uniformly located on the branches of TiO_2, so near-field dipolar interactions between adjacent particles were very strong. Therefore, the LSPR of Ag NPs can enhance the

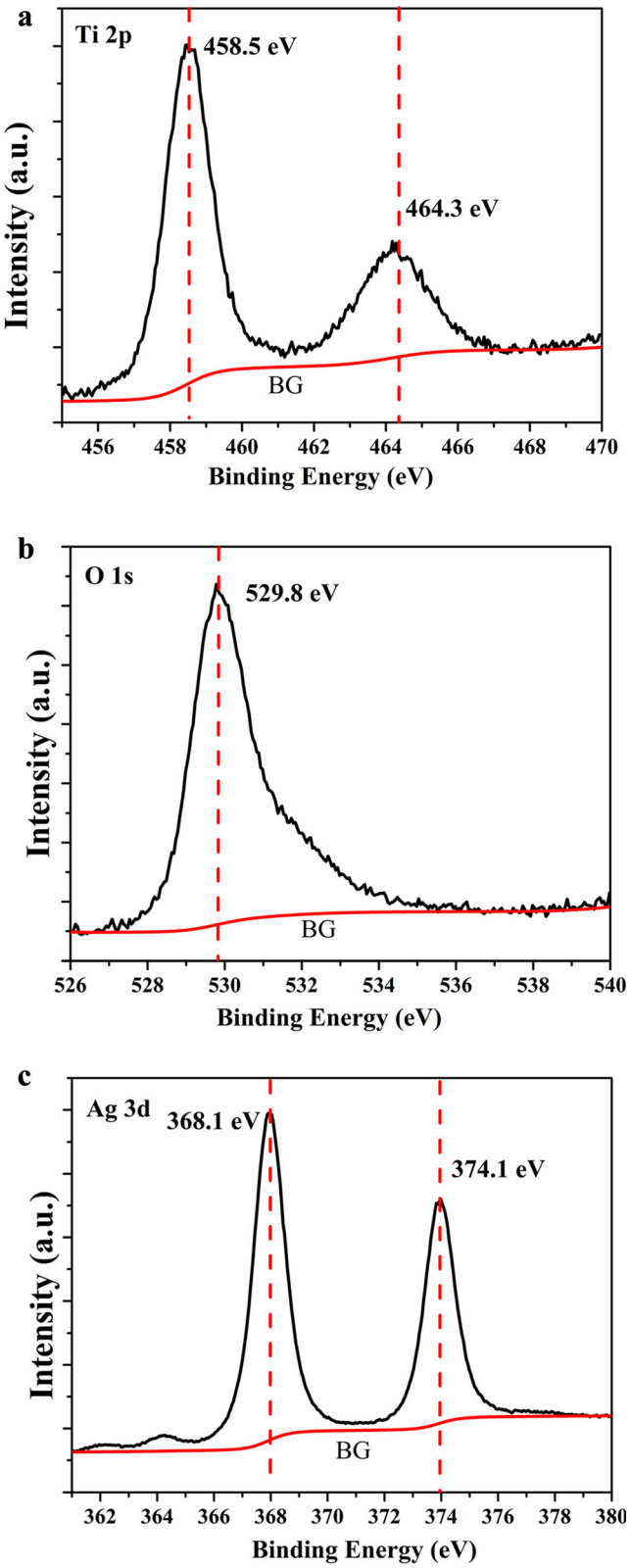

Fig. 4 XPS spectra of Ag(30s)/TiO_2: **a** high-resolution XPS of Ti 2p peaks, **b** high-resolution XPS of O 1s peaks, and **c** high-resolution XPS of Ag 3d peaks

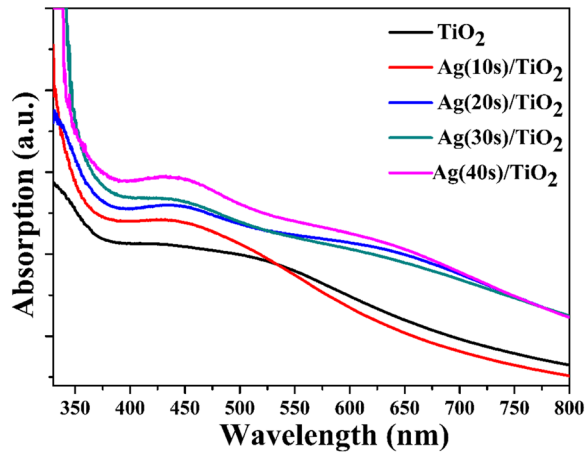

Fig. 5 UV-vis absorption spectra of TiO_2 and Ag/TiO_2 composite structure with different Ag deposition times

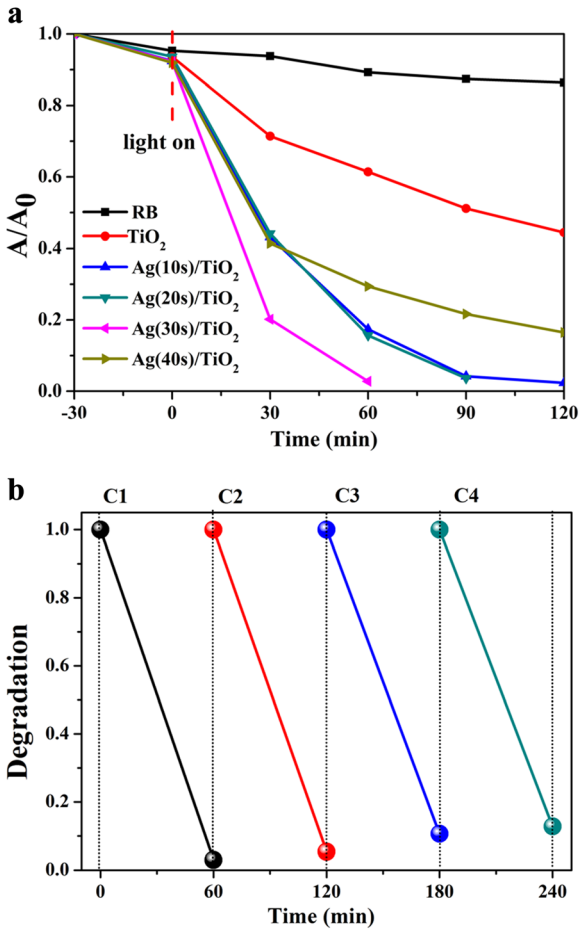

Fig. 6 **a** The typical degradation curve of RhB in the presence of TiO_2 and Ag/TiO_2 composite structure with different Ag deposition times under UV and visible light irradiation. **b** Degradability of different cycling runs for photocatalytic degradation of RhB of $Ag(30s)/TiO_2$ composite

local field near the surface of NPs as well as the giant field enhancement between adjacent particles [39, 46, 47]. Hence, there may be induced strong local electric field in the structure. The strong local electric field can increase the light capturing, and therefore boosts the generation of electron-hole pairs in Ag/TiO_2 composite, and hence improves the performance of photocatalysis. The typical Raman spectra of TiO_2, $Ag(10s)/TiO_2$, $Ag(20s)/TiO_2$, $Ag(30s)/TiO_2$, and $Ag(40s)/TiO_2$ are shown in Fig. 7. It can be observed that the Raman intensity of Ag/TiO_2 composites increases compared to that of pure TiO_2. The Raman scattering intensity increased with the increase of Ag deposition time and then decreased when the deposition time reaches 40 s, and the sample of $Ag(30s)/TiO_2$ shows the strongest Raman intensity. As is well known that Raman scattering intensity is proportional to the square of the intensity of a local field [47], Raman peak intensity enhancement is due to LSPR-mediated large near-field enhancement. The scattering and absorption cross-sections are separately proportional to R^6 and R^3 when the size of NPs is much smaller than the wavelength of light. As a result, for small particles (about <30 nm), the optical response dominates by absorption. Moreover, the absorption increases with the increased size of Ag NPs, it implies that the local electrical field induced by LSPR will increase with the increase of NP size. Therefore, the $Ag(30s)/TiO_2$ shows high enhancement factors of Raman scattering. However, the optical response dominates by scattering for larger particles [48, 49], so, the local field induced by LSPR of the Ag NPs of $Ag(40s)/TiO_2$ is weaker than that of other samples. On the other hand, due to the light scatter increase for $Ag(40s)/TiO_2$, the optical path increases, so the absorption of light can also increase. Therefore the $Ag(40s)/TiO_2$ also shows much higher photocatalytic performance than that of pure TiO_2. Based on our experiment results and literature, the boost generation of the electron-hole pairs due to the effect of LSPR is the critical factor to enhance the photocatalytic activity of TiO_2.

Table 1 The parameters on spectral distribution and relative intensity of the used mercury lamp in the photocatalytic tests

Wavelength (nm)	250	313	365	400	510	620	720
Relative intensity (%)	20	85	100	30	20	40	80

3) The electron transfer from Ag to TiO_2.
Figure 1c illustrates the possible charge transfer process in Ag/TiO_2 system. When TiO_2 is irradiated by light with energy higher than its band gap, valence electron is excited into the conduction band

Table 2 The degradation of RhB of TiO_2 and Ag/TiO_2 composite structure with different Ag deposition times under UV and visible light irradiation

Sample	TiO_2	Ag(10s)/TiO_2	Ag(20s)/TiO_2	Ag(30s)/TiO_2	Ag(40s)/TiO_2
Degradation time (min)	120	120	90	60	120
Degradation (%)	55	98	96	98	84
k value (min^{-1})	9×10^{-3}	3.5×10^{-2}	3.7×10^{-2}	6×10^{-2}	1.5×10^{-2}

and hole still in the valence. Valence holes accumulated to the surface and induced the surface hydroxyl radical · OH [50], then oxidated the decomposition of RhB. However, the generated electrons would transfer from the TiO_2 to Ag NPs because the work function of TiO_2 (4.2 eV [51]) is lower than that of Ag (4.52 to 4.74 eV [52]), and Ag NPs act as electron trap which effectively facilitate the separation of photogenerated carriers, thus improves the transfer efficiency of electron and hole pairs [53, 54]. The electrons on Ag NPs will be transferred to the absorbed oxygen and form superoxide, the formed superoxide is responsible for the reduction of organic RhB [55]. Thus, the Ag/TiO_2 structure can efficiently prevent the recombination of electron and hole, therefore improves the photocatalytic efficiency of TiO_2.

Conclusions

In summary, the high-performance plasmonic photocatalyst three-dimensional pine tree-like hierarchical TiO_2 nanotube array films loaded with Ag NPs were fabricated by a simple two-step process. A large number of uniform Ag NPs dispersed in the pin tree-like hierachical TiO_2, which effectively improved the light harvest, boosted the generation of electron and hole pairs, and notably improved the separation, transport, and electron-hole pairs with large specific surface area, significantly improved the photocatalytic performance under UV-visible light irradiation (seven times than pure TiO_2). Therefore, this research supplies an effective synthetic strategy for noble metal NP-modified three-dimensional hierarchical TiO_2, which will be of great significance for promising applications in the fields of environment and energy for high-efficiency light-energy conversion.

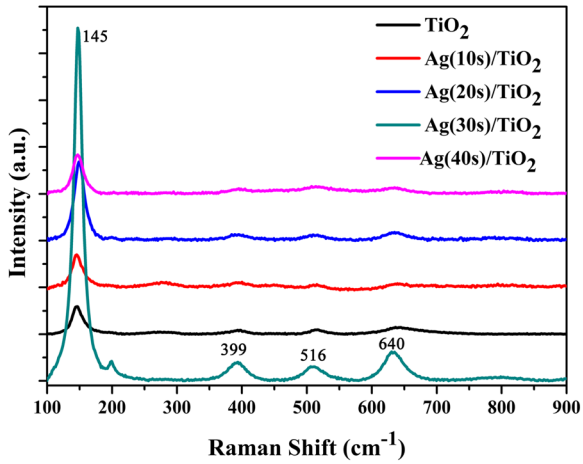

Fig. 7 Raman spectra of TiO_2 and Ag/TiO_2 composite structure with different Ag deposition times

Methods

Synthesis of Three-Dimensional Pine Tree-Like Hierarchical TiO_2 Nanotube Array Films

Three-dimensional tree-like TiO_2nanotube arrays were synthesized using a hydrothermal method. The details of the synthetic procedure were described by Roh et al. [56]. Briefly, 0.73 g of potassium titanium oxide oxalate dehydrates (PTO) was dissolved in 7-ml deionized water, and then, the mixed solution was added to 33-ml diethylene glycol (DEG) and stirred well. Fluorine-doped tin oxide (FTO) transparent conductive glass substrates were washed by isopropanol, chloroform, and deionized water successively. And then, a cleaned FTO was placed in a teflon-lined stainless steel autoclave filled with mixed solutions. The hydrothermal reactions temperature is 200 °C, and the reaction time is 11 h. After the reaction, the as-synthesized samples were washed with water more than once. After that, the as-prepared samples were annealed in air at 500 °C for 1 h to remove the residuary organic substance.

Preparation of Ag/TiO_2 Composites

Ag NPs were deposited on three-dimensional pine tree-like hierarchical TiO_2 nanotube array films by a magnetron sputtering system. The deposition rate of Ag is about 20 nm min^{-1}, and deposition time is 10, 20, 30, and 40 s, then obtained Ag NP-decorated three-dimensional pine tree-like hierarchical TiO_2 nanotube array films were named as Ag(10s)/TiO_2, Ag(20s)/TiO_2, Ag(30s)/TiO_2, and Ag(40s)/TiO_2.

Characterization

The morphology and microstructure of the sample was examined by SEM (S4800, Hitachi) operated at an acceleration voltage of 5 kV. The crystallinity and phase constitutions of all samples were analyzed with X-ray diffraction (XRD) (D8 Germany, Bruker Axs). The elemental chemical status and compositions were analyzed with X-ray photoelectron spectroscopy (XPS) using Mg Ka1, 2 (1253.6 eV) excitation. The Raman scattering spectra were analyzed by a micro-Raman system (LabRAM HR800, HORIBA JobinYvon, Paris, France). Ar laser (532.0 nm) is the

excitation source, and laser power was kept at 2.5 mW. The UV-vis absorption spectra of all samples were determined by UV-visible dual-beam spectrophotometer (Shimadzu UV 2550).

Photocatalytic Activity Measurement

The photocatalytic activity of the prepared sample with an area of about 6 cm^2 was evaluated by decolorization of 10-ml rhodamine B (RhB) solution with the concentration of 10 mg/L. Mercury lamplight as a UV and visible light source (spectral distribution and relative intensity of the mercury lamp in Table 1). The temperature was maintained at 18 °C in the process of photocatalytic reaction by equipping with a water circulation facility. Before irradiation, all samples were put into 10-ml RhB solution for 30 min in darkness in order to establish an adsorption/desorption equilibrium of RhB molecules on the surface of the photocatalysts. The degradation of RhB solution was determined by using an UV-vis spectrophotometer (Shimadzu UV 2550) at 554.0 nm. The time interval is 30 min, and the total reaction time was 2 h. As a comparison, the RhB solution was also measured under the same experimental conditions.

Abbreviations

D: Dimensional; DEG: Diethylene glycol; FTO: Fluorine-doped tin oxide; LSPR: Localized surface plasmon resonance; NPs: Nanoparticles; PTO: Potassium titanium oxide oxalate dehydrates; RhB: Rhodamine B; SEM: Scanning electron microscopy; XPS: X-ray photoelectron spectroscopy; XRD: X-ray diffraction

Acknowledgments

The authors are thankful to the NSFC (51371131, 11305056, and 61422407), Jiangsu Provincial Natural Science Foundation (BK20141217) and the Open Foundation of Hubei Collaborative Innovation Center for High-efficiency Utilization of Solar Energy (Grant Nos. HBSKFM2014013).

Funding

NSFC (51371131, 11305056, and 61422407), Jiangsu Provincial Natural Science Foundation (BK20141217) and the Open Foundation of Hubei Collaborative Innovation Center for High-efficiency Utilization of Solar Energy (Grant Nos. HBSKFM2014013).

Authors' contributions

JX participated in the material preparation and data analysis and drafted the manuscript. ZX, WQ, XG, and DH participated in the sample characterization. XX participated in its design and coordination. All authors read and approved the final manuscript.

Competing interests

The authors declare that they have no competing interests.

Author details

[1]Department of Physics and Key Laboratory of Artificial Micro- and Nano-Structures of Ministryof Education and Laboratory of Printable Functional Nanomaterials, Wuhan University, Wuhan 430072, People's Republic of China. [2]Hubei Collaborative Innovation Center for High-efficiency Utilization of Solar Energy and School of Electrical & Electronic Engineering, Hubei University of Technology, Wuhan 430068, People's Republic of China. [3]Su Zhou Institute of Wuhan University, Suzhou 215123, People's Republic of China.

Received: 5 November 2016 Accepted: 23 December 2016
Published online: 19 January 2017

References

1. Fujishima A, Honda K (1972) Electrochemical photolysis of water at a semiconductor electrode. Nature 238:37–38
2. Liu HY, Joo JB, Dahl M, Fu LS, Zeng ZZ, Yin YD (2015) Crystallinity control of TiO_2 hollow shells through resin-protected calcination for enhanced photocatalytic activity. Energy Environ Sci 8:286–296
3. Tan LL, Ong WJ, Chai SP, Yong ST, Mohamed AR (2014) Self-assembly of nitrogen-doped TiO_2 with exposed {001} facets on a graphene scaffold as photo-active hybrid nanostructures for reduction of carbon dioxide to methane. Nano Res 7:1528–1547
4. Hossain MA, Park J, Ahn JY, Park C, Kim Y, Kim SH, Lee D (2015) Investigation of TiO_2 nanotubes/nanoparticles stacking sequences to improve power conversion efficiency of dye-sensitized solar cells. Electrochim Acta 173:665–671
5. Li H, Yu H, Quan X, Chen S, Zhao H (2015) Improved photocatalytic performance of heterojunction by controlling the contact facet: high electron transfer capacity between TiO_2 and the {110} facet of $BiVO_4$caused by suitable energy band alignment. Adv Funct Mater 25:3074–3080
6. Bai S, Wang L, Chen X, Du J, Xiong Y (2015) Chemically exfoliated metallic MoS_2 nanosheets: a promising supporting co-catalyst for enhancing the photocatalytic performance of TiO_2 nanocrystals. Nano Res 8:175–183
7. Xiao FX, Hung SF, Miao J, Wang HY, Yang H, Liu B (2015) Metal-cluster-decorated TiO_2 nanotube arrays: a composite heterostructure toward versatile photocatalytic and photoelectrochemical applications. Small 11(5):554–567
8. Liu N, Schneider C, Freitag D, Hartmann M, Venkatesan U, Mîller J, Spiecker E, Schmuki P (2014) Black TiO_2 nanotubes: cocatalyst-free open-circuit hydrogen generation. Nano Lett 14:3309–3313
9. Zhou X, Liu N, Schmuki P (2014) Ar^+-ion bombardment of TiO_2 nanotubes creates co-catalytic effect for photocatalytic open circuit hydrogen evolution. Electrochem Commun 49:60–64
10. Asahi R, Morikawa T, Irie H, Ohwaki T (2014) Nitrogen-doped titanium dioxide as visible-light-sensitive photocatalyst: designs, developments, and prospects. Chem Rev 114:9824–9852
11. Zhou X, Häublein V, Liu N, Nguyen NT (2016) TiO_2 nanotubes: nitrogen-ion implantation at low dose provides noble-metal-free photocatalytic H_2-evolution activity. Angew Chem Int Ed 55:3763–3767
12. Priebe JB, Radni KJ, Lennox AJJ, Pohl M, Karnahl M, Hollmann D, Grabow K, Bentrup U, Junge H, Beller M, Brîckner A (2015) Solar hydrogen production by plasmonic Au–TiO_2 catalysts: impact of synthesis protocol and TiO_2 phase on charge transfer efficiency and H_2 evolution rates. ACS Catal 5:2137–2148
13. Liao JY, Lei BX, Chen HY, Kuang DB, Su CY (2012) Oriented hierarchical single crystalline anatase TiO_2 nanowire arrays on Ti-foil substrate for efficient flexible dye-sensitized solar cells. Energy Environ Sci 5:5750–5757
14. Giordano F, Abate A, Baena JPC, Saliba M et al (2016) Enhanced electronic properties in mesoporous TiO_2 via lithium doping for high-efficiency perovskite solar cells. Nat Commun 7:10379
15. Wang H, Wang B, Yu J, Hu Y, Xia C, Zhang J, Liu R (2014) Significant enhancement of power coversion efficiency for dye sensitized solar cell using 1D/3D network nanostructures as photoanodes. Sci Rep 5(9305):1–9
16. Li Z, Ding Y, Mo L, Hu L, Wu J, Dai S (2015) Fine tuning of nanocrystal and pore sizes of TiO_2 submicrospheres toward high performance dye-sensitized solar cells. ACS Appl Mater Interfaces 7:22277–22283
17. Wang C, Yin L, Zhang L, Qi Y, Lun N, Liu N (2010) Large scale synthesis and gas-sensing properties of anatase TiO_2 three-dimensional hierarchical nanostructures. Langmuir 26:12841–12848
18. Lou Z, Li F, Deng J, Wang LL (2013) Branch-like hierarchical heterostructure (α-Fe_2O_3/TiO_2): a novel sensing material for trimethylamine gas sensor. ACS Appl Mater Interface 5(23):12310–12316
19. Yang G, Xiao T, Sloan J, Li G, Yan Z (2011) Low-temperature synthesis of visible-light active fluorine/sulfur co-doped mesoporous TiO_2 microspheres. Chem Eur J 17:1096
20. Bisquert J, Cahen D, Hodes G, RuhleS ZA (2004) Physical chemical principles of photovoltaic conversion with nanoparticulate, mesoporous dye-sensitized solar cells. J Phys Chem B 108:8106–8118
21. Zhu K, Neale NR, Miedaner A, Frank AJ (2007) Enhanced charge-collection efficiencies and light scattering in dye-sensitized solar cells using oriented TiO_2 nanotubes arrays. Nano Lett 7:69–74
22. Baker DR, Kamat PV (2009) Photosensitization of TiO_2 nanostructures with CdS quantum dots: particulate versus tubular support architectures. Adv Funct Mater 19:805–811

23. Jiu J, Isoda S, Wang F, Adachi M (2006) Dye-sensitized solar cells based on a single-crystalline TiO_2 nanorod film. J Phys Chem B 110:2087–2092
24. Wang J, Lin Z (2008) Freestanding TiO_2 nanotube arrays with ultrahigh aspect ratio via electrochemical anodization. Chem Mater 20:1257–1261
25. Joshi RK, Schneider JJ (2012) Assembly of one dimensional inorganic nanostructures into functional 2D and 3D architectures. Synthesis, arrangement and functionality. ChemSocRev 41:5285–5312
26. Chen Q, Chen C, Ji H, Ma W, Zhao J (2013) Surfactant-additive-free synthesis of 3D anatase TiO_2 hierarchical architectures with enhanced photocatalytic activity. RSC Adv 3:17559
27. Liu J, Yang SL, Wu W, Tian QY, Cui SY, Dai ZG, Ren F, Xiao XH, Jiang CZ (2015) 3D Flowerlike α-Fe_2O_3@TiO_2core – shell nanostructures: general synthesis and enhanced photocatalytic performance. ACS Sustainable Chem Eng 3:2975–2984
28. Pathak P, Gupta S, Grosulak K, Imahori H, Subramanian V (2015) Nature-inspired tree-like TiO_2 architecture: a 3D platform for the assembly of CdS and reduced graphene oxide for photoelectrochemical processes. J Phys Chem C 119:7543–7553
29. Jiang TT, Jia CC, Zhang LC, He SR, Sang YH, Li HD, Li YQ, Xu XH, Liu H (2015) Gold and gold-palladium alloy nanoparticles on heterostructured TiO_2 nanobelts as plasmonic photocatalysts for benzyl alcohol oxidation. Nanoscale 7:209–217
30. Awazu K, Fujimaki M, Rockstuhl C, Tominaga J, Murakami H, Ohki Y, Yoshida N, Watanabe T (2008) A plasmonic photocatalyst consisting of silver nanoparticles embedded in titanium dioxide. J Am Chem Soc 130:1676–1680
31. Kumar MK, Krishnamoorthy S, Tan LK, Chiam SY, Tripathy S, Gao H (2011) Field effects in plasmonic photocatalyst by precise SiO_2 thickness control using atomic layer deposition. ACS Catal 1:300–308
32. Zhang XG, Wang B, Wang XZ, Xiao XX, Dai ZG, Wu W, Zheng JF, Ren F, Jiang CZ (2015) Preparation of M@ $BiFeO_3$nanocomposites (M = Ag, Au) bowl arrays with enhanced visible light photocatalytic activity. J Am Ceram Soc 98:2255–2263
33. Pu YC, Wang G, Chang KD, Ling Y, Lin YK, Fitzmorris BC, Liu CM, Lu X, Tong Y, Zhang JZ, Hsu YJ, Li Y (2013) Au nanostructure-decorated TiO_2 nanowires exhibiting photoactivity across entire UV-visible region for photoelectrochemical water splitting. Nano Lett 13:3817–3823
34. Kerker M (1985) The optics of colloidal silver: something old and something new. J Colloid Interface Sci 105:297–314
35. Sun L, Li J, Wang CL, Li SF, Lai YK, Chen HB, Lin CJ (2009) Ultra sound aided photochemical synthesis of Ag loaded TiO_2 nanotube arrays to enhance photocatalytic activity. J Hazard Mater 171:1045–1050
36. Fan Z, Meng F, Zhang M, Wu Z, Sun Z, Li A (2016) Solvothermal synthesis of hierarchical TiO_2 nanostructures with tunable morphology and enhanced photocatalytic activity. Appl Surf Sci 360:298–305
37. Zhang WF, He YL, Zhang MS, Yin Z, Chen Q (2000) Raman scattering study on anatase TiO_2 nanocrystals. J Phys D Appl Phys 33:912–916
38. Samara GA, Peercy PS (1973) Pressure and temperature dependence of the static dielectric constants and Raman spectra of TiO_2 (Rutile). Phys Rev B 7:1131–1148
39. Biteen JS, Lewis NS, Atwater HA (2006) Spectral tuning of plasmon-enhanced silicon quantum dot luminescence. Appl Phys Lett 88(131109):1–3
40. Price NJ, Reitz JB, Madix RJ, Solomon EJA (1999) A synchrotron XPS study of the vanadia–titania system as a model for monolayer oxide catalysts. J Electron Spectrosc Relat Phenom 257:98–99
41. Yu J, Yu H, Cheng B, Zhou H, Zhao J (2006) Enhanced photocatalyticactivity of TiO_2 power (P25) by hydrothermal treatment. J Mol Catal A Chem 253:112–118
42. Yang LB, Jiang X, Ruan WD, Yang XJ, Zhao B, Xu WQ, Lombardi JR (2009) Charge-transfer-induced surface-enhanced raman scattering on Ag-TiO_2 nanocomposites. J Phys Chem C 113:16226
43. Linsebigler AL, Lu GQ, Yates JT Jr (1995) Photocatalysis on TiO_2 surfaces: principles, mechanisms, and selected results. Chem Rev 95:735–758
44. Al-Ekabi H, Serpone N (1988) Kinetics studies in heterogeneous photocatalysis. I. Photocatalytic degradation of chlorinated phenols in aerated aqueous solutions over titania supported on a glass. J Phys Chem 92:5726–5731
45. Choi J, Kang G, Park T (2015) A competitive electron transport mechanism in hierarchical homogeneous hybrid structures composed of TiO_2nanoparticles and nanotubes. Chem Mater 27:1359–1366
46. Xie K, Sun L, Wang C, Lai Y, Wang M, Chen H, Lin C (2010) Photoelectrocatalytic properties of Ag nanoparticles loaded TiO_2 nanotube arrays prepared by pulse current deposition. Electrochim Acta 55:7211–7218
47. Garcia-Vidal FJ, Pendry JB (1996) Collective theory for surface enhanced Raman scattering. Phys Rev Lett 77:1163–1166
48. Evanoff DD Jr, Chumanov G (2005) Synthesis and optical properties of silver nanoparticles and arrays. Chem Phys Chem 6:1221–1231
49. Rycenga M, Cobley CM, Zeng J, Li W, Moran CH, Zhang Q, Qin D, Xia Y (2011) Controlling the synthesis and assembly of silver nanostructures for plasmonic applications. Chem Rev 111:3669–3712
50. Alberic RM, Jardim WF (1997) Photocatalytic destruction of VOCs in thegas-phase using titanium dioxide. Appl Catal B-Environ 14:55–68
51. Tan TY, Yip CK, Beydoun D, Amal R (2003) Effects of nano-Ag particles loading on TiO_2 photocatalytic reduction of selenate ions. Chem Eng J 95:179–186
52. Fang YJ, Sha J, Wang ZL, Wan YT, Xia WW, Wang YW (2011) Behind the change of the photoluminescence property of metal-coated ZnO nanowire arrays. Appl Phys Lett 98:033103
53. Subramanian V, Wolf EE, Kamat PV (2004) Catalysis with TiO_2/gold nanocomposites. Effect of metal particle size on the Fermi level equilibration. J Am Chem Soc 126:4943
54. Hirakawa T, Kamat PV (2005) Charge separation and catalytic activity of Ag@ TiO_2 core-shell composite clusters under UV-irradiation. J Am Chem Soc 127:3928
55. Miyauchi M, Nakajima A, Hashimoto K, Watanabe T (2000) A highly hydrophilic thin film under 1 μW/cm^2 UV illumination. Adv Mater 12:1923–1927
56. Roh DK, Chi WS, Jeon H, Kim SJ, Kim JH (2014) High efficiency solid-state dye-sensitized solar cells assembled with hierarchical anatase pine tree-like TiO_2 nanotubes. Adv Funct Mater 24:379–386